1.

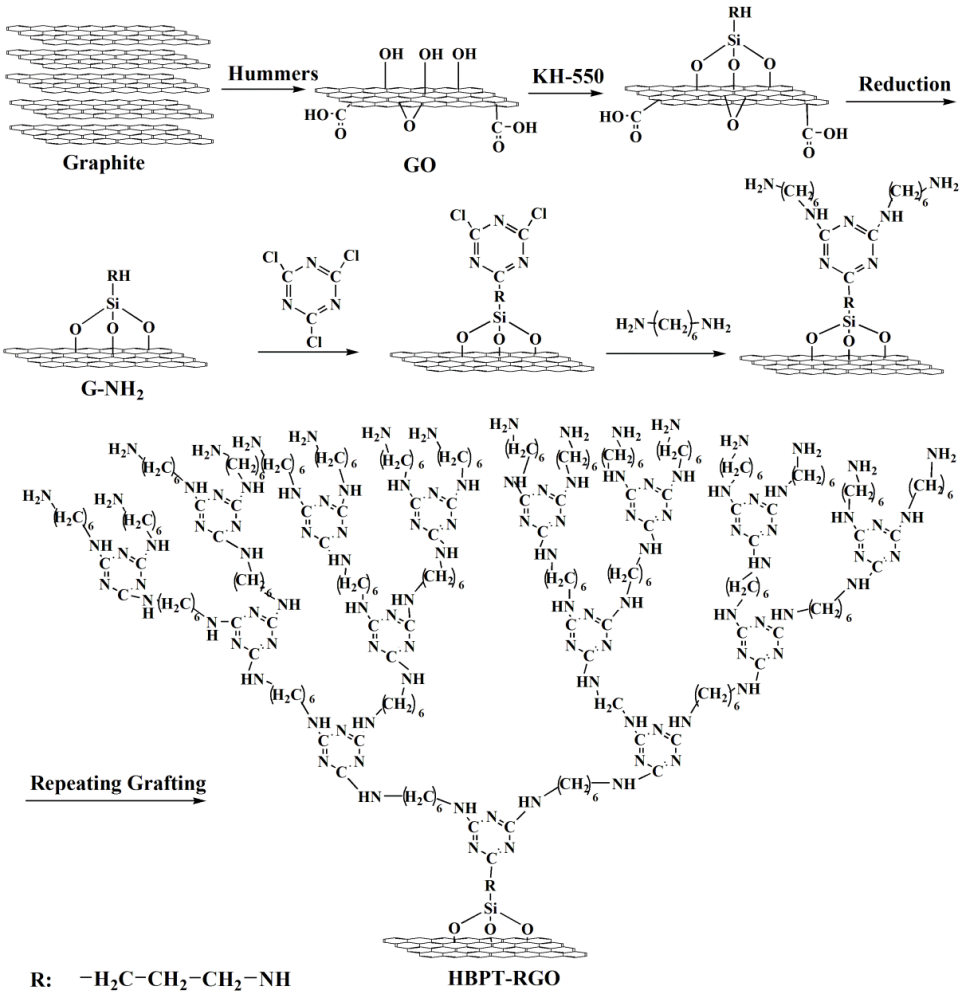

Fig. S1 The Chemical route for the preparation of HBPT-RGO.

2. Determination of the ratio of grafting

The KH-550 (or polytriazine polymers) content of G-NH_2 (or the HBPT-RGO) was determined by use of a thermogravimetric analyzer (TGA; Shimadzu TGA-50) to further research the grafting rate of KH-550 (or polytriazine polymers) on the surface of reduced graphene oxide. The ratio of grafting was determined by the following equation:

$$\text{Grafting (\%)} = (A / B) \times 100$$

Where A is the weight of KH-550 (or polytriazine) grafted and B the weight of the graphene oxide charged after reduction. The weight of KH-550 (or polytriazine) grafted onto the graphene were determined as the weight lost when G-NH_2 (or HBPT-RGO) was heated to 800 ^{o}C.

Amino groups were introduced onto reduced graphene oxide surface by hydrolytic condensation reaction. In this study, the G-NH_2 containing 0.66 mmol/g of amino groups were used for the grafting reaction. Then, the polytriazine was introduced onto the reduced graphene oxide surface. It was shown in Table 1 that polytriazine moieties was successfully introduced onto graphene surface. Though the percentage of polytriazine polymers grafted onto graphene surface exceeded 116%, it was considerably smaller than the calculated value. This may have been due to the fact that the chains grafted onto the graphene surface interfered with the propagation of the hyperbranched polymers because of steric hindrance.

Table S1 Grafting of KH-550 and polytriazine polymers onto reduced graphene oxide surface

Samples	Grafting (%)	
	Observed	Calculated
G-NH_2	14.6	_
HBPT-RGO	116	1996

3.

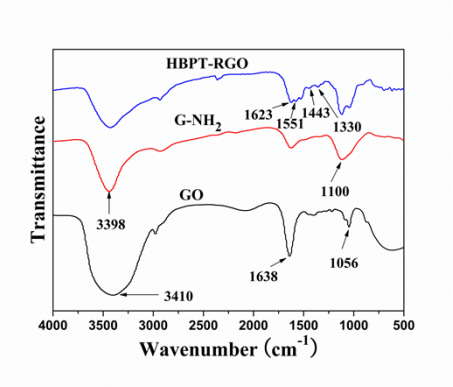

Fig. S2 FTIR spectra of GO, G-NH_2, and HBPT-RGO.

Fourier Transform Infrared (FTIR) Spectra. Each sample was pressed into a pellet with KBr, which was then put into a Prostar LC240 infrared spectrometer (Agilent Technologies, Palo Alto, USA) for getting the FTIR spectrum between 500 and 4000 cm^{-1} at a resolution of 2 cm^{-1}. In Fig. S2, the peaks at 3430, 1638 and 1056cm^{-1} correspond to -OH, C=C and C-O stretching vibration of GO, respectively. After grafting with KH-550, the new typical peaks appeared (the peak at 1100cm^{-1} belongs to Si-O-C stretching vibrations and the peak at 3388cm^{-1} belongs to N-H stretching vibrations), indicating that KH-550 had been successfully grafted onto the graphene. In the spectrum of HBPT-RGO, the bands at 1443, 1551 and 1623 cm^{-1} are assigned to the skeleton vibration of the triazine ring and the band at 1330cm^{-1} was assigned to the C-N stretching vibration of the carbon atoms of triazine rings linked with the -NH-, implying that triazine rings were grafted onto graphene via the substitution reaction between G-NH_2. No absorption at 848 cm^{-1} in the spectrum of HBPT-RGO, which could be attributed to the lower steric hindrance of cyanuric chloride and that the Cl atoms in cyanuric chloride were almost substituted by the -NH_2 groups of HMD. The above results indicated that hyperbranched polytriazine had been successfully grafted onto the graphene backbone.

4.

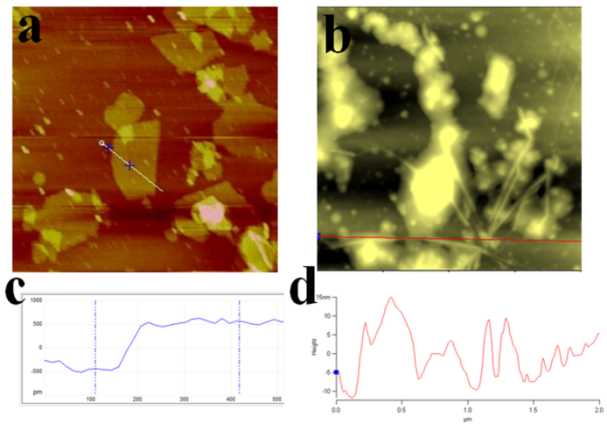

Fig. S3 (a) AFM image of GO on the INNOVA, 2×2 μm, (b) AFM image of HBP-RGO on the MFP-3D-SA, 2×2 μm, (c) height line in the image of GO and HBP-RGO (d).

The HBP-RGO was dispersed in water, transferred to the silicon wafer, the solvent evaporation with N_2 purging and then mounted on the AFM scan head to observe its microstructure (AFM images of GO on the INNOVA and HBP-RGO on the MFP-3D-SA). Fig. S3a showed a scan over an area of 2 μm × 2 μm. As can be seen that many large single-layer GO sheets can be seen clearly. The resulting distribution of the measured relative thickness gives the histogram reported in Fig. S3c. The average thickness is less than 1 nm, which showed that the GO what we had prepared is single-layer. Fig. S3b showed a scan over an area of 2 μm × 2 μm of HBP-RGO. The resulting distribution of the measured relative thickness gave the histogram reported in Fig. S3d. The average thickness is less than 15 nm. It can be seen in Fig. S3b, the addends had clear branched structure. Comprehensive the above characterization results, it could be concluded that hyperbranched polytriazine had been grafted onto the graphene as designed. Whereas, the reactive functional groups between the graphene sheets might be have a certain reaction, resulting in crosslinking phenomenon. This might be due to steric hindrance and the low reactivity of grafting process.

5.

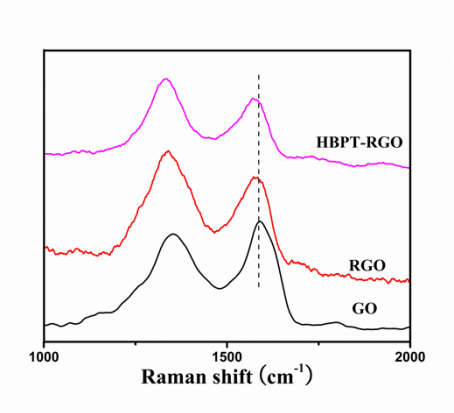

Fig. S4 Raman spectra of GO, RGO, and HBPT-RGO.

Raman spectroscopy is one of the best tools for analysis carbon material. Raman spectrum of GO sample reveals both G (the E_{2g} phonon mode of sp^2 carbon atoms) and D (the breathing mode of *k*-point mode of A_{1g} symmetry) bands at 1588 and 1353cm^{-1}, respectively (Fig. S4). When compared with GO, G bands of HBPT-RGO shifted to a low-wavelength range, indicating the significantly decrease of oxygen-containing functionalized groups on the graphene backbone. D band and G band intensity value relative I_D / I_G in the sample is inversely proportional to the size of the graphite crystallite size. For the RGO, the intensity ratio (I_D/I_G) was 1.12. As for the HBPT-RGO sample, the intensity ratio (I_D/I_G) increased to 1.42, respectively. The increased ratios showed that the number of defects in the graphene sheets increased after grafting of hyperbranched polymers. That was to say, the hyperbranched polymers had been grafted onto the graphene sheets.

6.

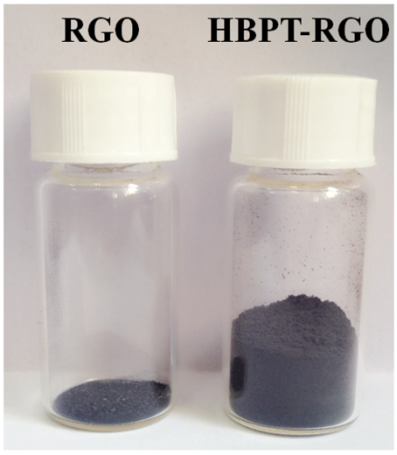

Fig. S5 Digital photos of 0.1g RGO (the left one) and 0.1g HBPT-RGO (the right one), respectively.

It could be seen in Fig. S5, the graphene turned fluffy after grafting the hyperbranched polytriazine. This was attributed to the existence of hyperbranched polytriazine on the graphene surface could prevent the aggregation and restacking of graphene sheets.

7.

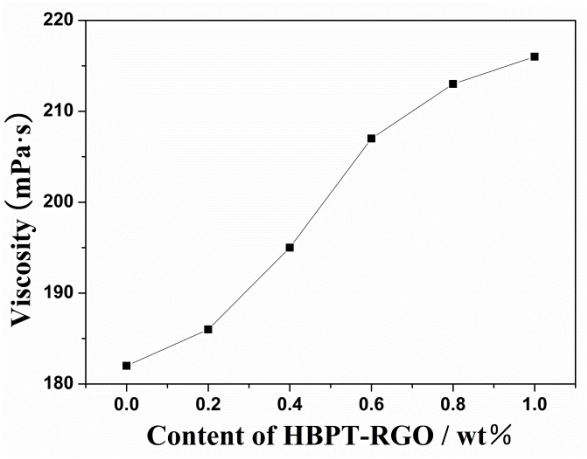

Fig. S6 The viscosity of the composites with different content RGO.

It could be seen in Fig. S6, the viscosity of the HBPT-RGO/BMI-BA melts at 135 °C (200 rpm) for 60 min. It could be seen in Fig. S6, the viscosity of melt increased continuously with the addition of HBPT-RGO. As we all know, the changes of fluid viscosity have much to do with the formation of some structure within the fluid.[1] There was a wealth of terminal amino groups on the HBPT-RGO surface, which could react with the carbon-carbon double bonds of BMI. With the addition of HBPT-RGO, the degree of crosslinking of BMI-BA increased and then the viscosity of melt increased.[2] Overall, the viscosity of HBPT-RGO/BMI-BA melt remained at a comparatively low level, which benefited the dispersion of the nanoparticles in the system and the cast molding of composites. This might be attributed to the lower loading of the HBPT-RGO.

[1] F. Bueche, *J. Chem. Phys*., 1952, **2**0, 1959.

[2] M. Sumita, H. Abe, H. Kayaki, K. Miyasaka, *J. Macromol. Sci. B*., 1986, **25**, 171.

8.

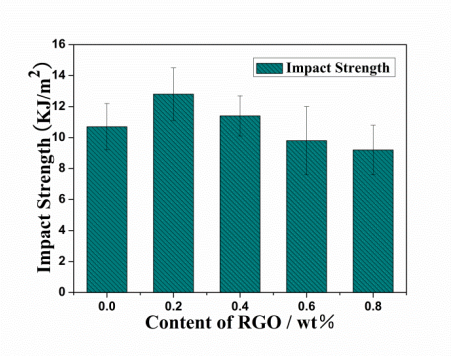

Fig. S7 The impact strength of the composites with different content RGO.

The impact strength of the composites with different content of RGO was shown in Fig. S7. It could be seen that suitable amount of RGO could properly improve the impact strength of BMI-BA resin. However, when the amounts of RGO were further increased, unfortunately, the impact strength of composites decreased, and even lower than the neat BMI-BA composites. This phenomenon could be explained that RGO showed poor compatibility with the BMI-BA resin and excessive RGO agglomerated in the matrix, thus the advantages of the RGO could not be fully realized.

9.

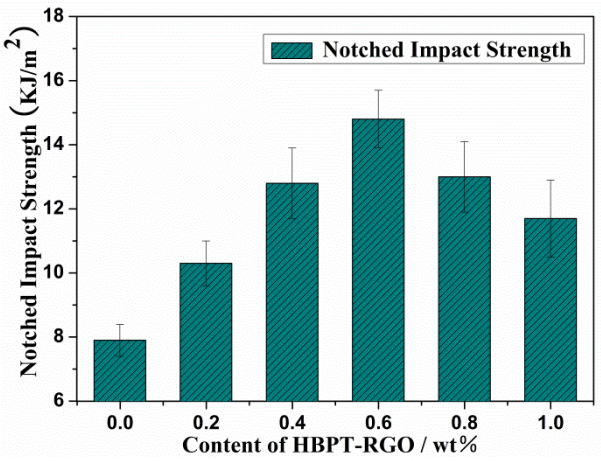

Fig. S8 The notched impact strength of the composites with different content HBPT-RGO.

To further study the toughness of the HBPT-RGO/BMI-BA composites, the notched impact strength of that was investigated (See Fig. S8). The notched impact strength of HBPT-RGO/BMI-BA composites was obtained according to GB/T2567-2008. The samples dimension for notched impact test were (80±0.2)×(10±0.2)×(4.0±0.2) mm^3. The radius of the arc gap at the bottom was 0.25±0.05 mm. It could be seen that a small addition of HBPT-RGO could obviously improve the notched impact strength of HBPT-RGO/BMI-BA composites, the notched impact strength of that reached the maximum value of 14.8 kJ/m^2 at 0.6 wt% HBPT-RGO. Then the notched impact strength of HBPT-RGO/BMI-BA composites decreased with the increase in HBPT-RGO loading, which was considered that uneven distribution and agglomeration of HBPT-RGO make it easy to form stress concentration when HBPT-RGO loading increased to a certain extent. The notched impact strength of HBPT-RGO/BMI-BA composites was lower than the unnotched impact strength of the HBPT-RGO/BMI composites at the same loading. This phenomenon was attributed to that the shear stress concentration in different positions of the testing samples during the impact process. For the unnotched impact test, the shear stress concentration in the middle of the samples during the impact process. For the notched impact test, the shear stress concentration in the notch of the samples during the impact process. The notched impact strength of HBPT-RGO/BMI-BA composites were same as the unnotched impact strength of those, which confirmed that the toughness of BMI-BA could be improved with the suitable addition of HBPT-RGO.

10.

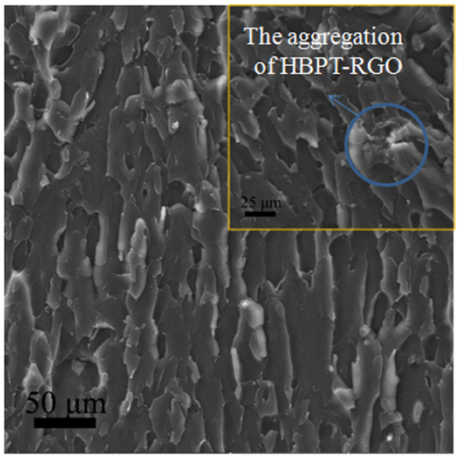

Fig. S9 SEM picture of fracture surface taken from the composite with 1.0 wt% HBPT-RGO in impact test.

To further research the fracture characteristics of materials, the fracture surfaces of the composite filled with 1.0 wt% HBPT-RGO taken from impact tests were explored. It could be seen that there was few number of aggregation in the picture (See Fig. S9). This phenomenon could be explained that excessive HBPT-RGO agglomerated in the resin matrix.

11.

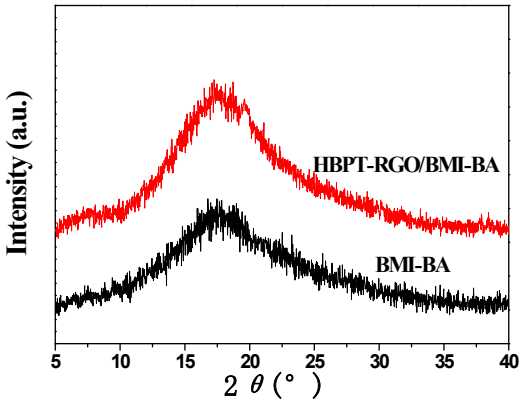

Fig. S10 XRD patterns of neat BMI-BA and HBPT-RGO/BMI-BA composites.

Figure S10 showed XRD patterns of neat BMI-BA and its composites with HBPT-RGO. A wide diffraction from 5 to 35° was observed in both of the curves, which represented the scattering of cured BMI-BA molecules. Compared to the neat BMI-BA, a low and weak peak appeared around 7.5° in the XRD pattern of HBPT-RGO/BMI-BA, which might be associated with the HBPT-RGO that was not completely reduced. The lower diffraction at 19.8° was associated with the HBPT-RGO, while that of it move to a lower degree compared to the diffraction peak of HBPT-RGO (See Fig. 2 in the manuscript). This phenomenon implied that a higher degree of dispersion and exfoliation of graphene through the preparation of HBPT-RGO/BMI-BA composites. Therefore the surface modification of HBPT-RGO by long chain molecules builds up a covalently bonded interface with the matrix, promoting the dispersion and delamination of graphene sheets.[1]

[1] Q. Meng, J. Jin, R. Wang, H. C. Kuan, J. Ma, N. Kawashima, C. H. Wang, *Nanotechnology*,2014, **25**, 125707.

12.

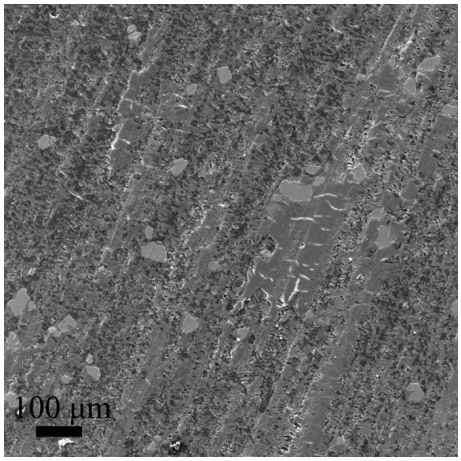

Fig. S11 SEM images of worn surface of 0.6 wt% RGO/BMI-BA composite.

Fig. S11 showed that the worn surface of 0.6 wt% RGO/BMI-BA. It was rough and many scratching grooves and slots were also found, which reflected that the composite had relatively poor wear resistance in its sliding against the steel counterpart. There were also some smooth scales that could be seen on the worn surface, which attributed to the RGO near the surface of resin matrix could be precipitated and act as a self-lubricating "carbon film" on the worn surface of composites during the wear process. Nevertheless, the distribution of scales was not uniform which mainly attributed to the aggregation of RGO in the resin matrix.

13.

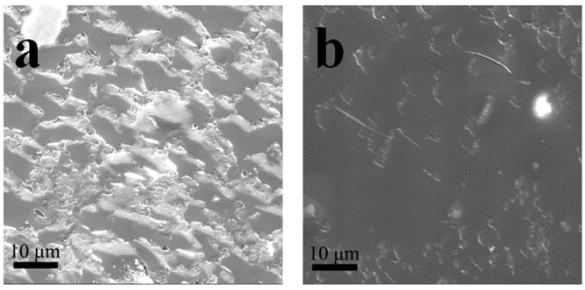

Fig. S12 SEM images of worn surfaces taken from 0.2 wt% HBPT-RGO/BMI-BA (a) and 1.0 wt% HBPT-RGO/BMI-BA composites (b) after friction tests.

Fig. S12a showed that the worn surface of 0.2 wt% HBPT-RGO/BMI-BA. It was rough and many scratching grooves and slots were also found, which reflected that the composite had relatively poor wear resistance in its sliding against the steel counterpart. There were also some smooth scales that could be seen on the worn surface, which attributed to the HBPT-RGO near the surface of resin matrix could be precipitated and act as a self-lubricating “carbon film” on the worn surface of composite during the wear process. Compared to Fig. S12a, fewer cracks and slots could be seen on the worn surface of 1.0 wt% HBPT-RGO/BMI-BA composite in Fig. S12b. It seemed more compact and less apt to form debris from the matrix, which might be related with the superior tribological property of graphene and better interfacial adhesion between HBPT-RGO and BMI-BA matrix, which was the characteristic of abrasive wear mechanism. This phenomenon indicated that the anti-wear ability of the composites was reinforced by HBPT-RGO. Some particles could be seen on the worn surface of HBPT-RGO/BMI-BA composite, which was attributed to the aggregation of the excessive amounts of HBPT-RGO in the resin matrix. Therefore, advantages of the HBPT-RGO could not be fully realized due to the excessive amounts of the fillers which would result in the increase of the friction coefficient and volume wear rate of the composites.

14.

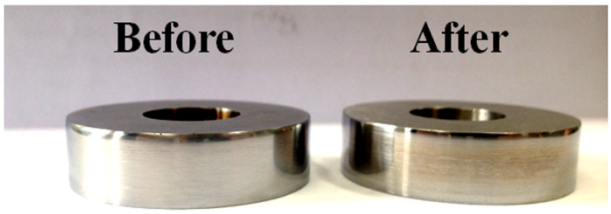

Fig. S13 Digital photos of counterpart steel ring friction before (a) and after (b) the friction tests of HBPT-RGO/BMI-BA composite.

In order to further prove the existence of the “carbon film”, we provided the digital photos of counterpart steel ring before (Fig. S13a) and after (Fig. S13b) the friction tests of HBPT-RGO/BMI-BA composite. It could be seen that thin film was formed on the counterpart steel ring surface after the friction test, which was attributed to the fact that the HBPT-RGO in the matrix near the surface was exposed and acted as the lubricating thin “carbon film” on the counterpart steel ring surface.

15.

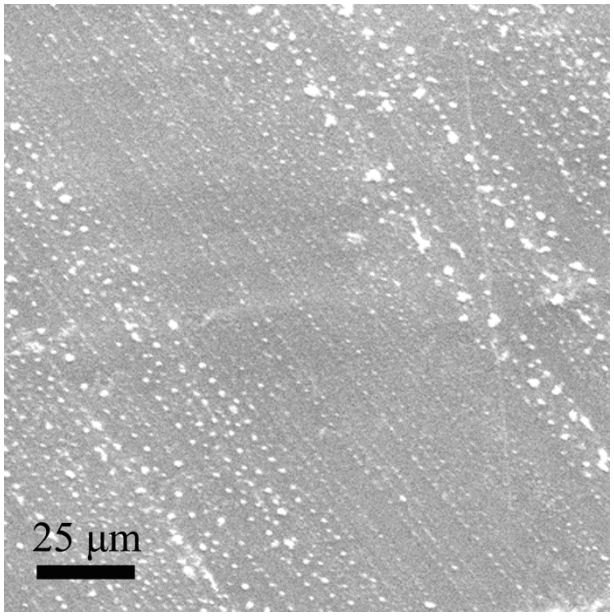

Fig. S14 Microphotograph of the counterpart steel ring surface of 0.6 wt% HBPT-RGO/BMI-BA composite.

As shown in Fig.14, a smooth film with lots of notches and small particles were found on the counterpart steel ring surface for 0.6 wt% HBPT-RGO/BMI-BA after friction test, which indicated that HBPT-RGO near the surface of resin matrix could be precipitated and act as a self-lubricating transfer film on the surface of the counterpart steel ring during the wear process. The small particles could be squeezed into flaky particles, and then formed a thin and continuous transfer film on the counterpart steel ring surface. Meanwhile, the transfer film inhibited the transfer of resin to the worn surface of composites and the counterpart steel ring during the wear process, thereby decreasing the friction coefficient and wear rate of the resin composites.

16.

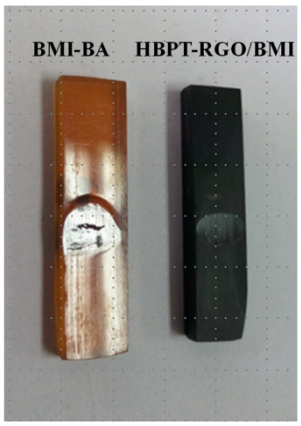

Fig. S15 Digital photos of neat BMI-BA (a) and 0.6 wt% HBPT-RGO/BMI-BA(b) samples after the friction tests under high load.

In order to confirm the presence of HBPT-RGO was advantageous to the heat transfer during the worn process, we also studied the wear surface photographs of BMI-BA and 0.6 wt% HBPT-RGO/BMI-BA composites under dry sliding condition (MM-200, load 294 N, speed 400 rpm/min) for 25 min. It could be seen that the neat BMI-BA had a visible deformation after friction test (See Fig. S15). Meanwhile, the wear mass loss of neat BMI-BA was obviously higher than that of 0.6 wt% HBPT-RGO/BMI-BA composite. This phenomenon might be attributed to the good thermal conduction and self-lubricating properties of HBPT-RGO. During the worn process, tremendous heat would generate on the wear surface, where the structure of composites might be destroyed under high-temperature. While, friction heat in the composites could be transmit efficiently because of good thermal conduction of HBPT-RGO, resulting in inhibition of destruction caused by high-temperature [1]. This study indicated that the anti-wear ability of composites was reinforced by HBPT-RGO.

[1] B. L. Pan, S. P. Zhang, W. Z. Li, J. Zhao, J. L. Liu, Y. Q. Zhang, and Y. Z. Zhang, *Wear*, 2012, **294**, 395.

17.

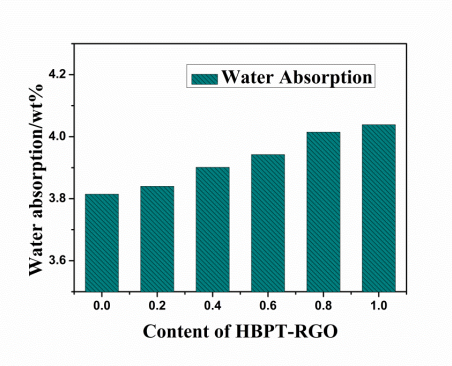

Fig. S16 The water absorption of the composites with different content HBPT-RGO.

The water absorption of the composites with different content of HBPT-RGO was shown in Fig. S16. It could be seen that the water absorption increased continuously with the addition of HBPT-RGO, which was mainly attributed to the HBPT-RGO was rich in hydrophilic amino groups. However, the changes were small, less effect on the properties of composites.

18.

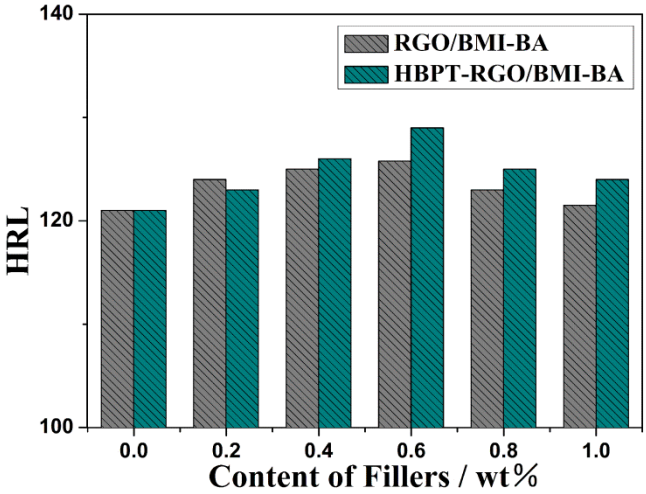

Fig. S17 The hardness of the composites with different content of RGO and HBPT-RGO.

Hardness was a measure of the material resistance to various kinds of permanent shape change when a force was applied and the hardness of material was closely related with tribological properties [1]. In this study, the dependency of the hardness of the RGO/BMI-BA and HBPT-RGO/BMI-BA composites on the content of the fillers was shown in Fig. S17. It could be observed that similar variation tendency in the hardness of the RGO/BMI-BA and HBPT-RGO/BMI-BA composites when the content was lower than 0.6 wt%. However, when the content of RGO was further increases, the hardness of the composite decreased, but was still higher than the BMI-BA resin. This was attributed to the increasing of the addition amount, more graphene aggregation in the resin, resulting in more small voids in the material, which decreased the hardness. While, when the filler content was 0.2 wt%, the hardness value of RGO/BMI was higher than that of the HBPT-RGO/BMI composites. This phenomenon could be attributed to the reduction and functionalization steps in preparing the HBPT-RGO, which decreased the mechanical strength of graphene, so the strength and dispersion of nanofillers corporately leaded to the result that HBPT-RGO/BMI-BA composites presented this hardness performance.

[1] A. Leyland, A. Matthews, *Wear,* 2000, **246**, 1.